Supporting Information

Bioorthogonal Conjugation of NIR Luminescent Gold Nanoclusters with Multifunctional Polymers: Insights into Binding efficiency, Kinetics, and Optical Properties

Furhan Abdul Rezak,[a,b] Pelin Catal,[c] Lola Mantout,[c] Fernande Da Cruz,[c] Didier Boturyn,[b]

Jean-Luc Coll,[a] Arnaud Favier,[c] Galina V. Dubacheva,[b*] Xavier Le Guével[a*]

[a] *Institut pour l'Avancée des Biosciences (IAB), Université Grenoble Alpes, INSERM U1209, CNRS-UMR 5309, 38700 Grenoble, France.*

[b]*Département de Chimie Moléculaire (DCM), Université Grenoble Alpes, CNRS-UMR 5250, 38000 Grenoble Cedex 9, France.*

[C] *Universite Claude Bernard Lyon 1, INSA Lyon, Université Jean Monnet, CNRS UMR 5223, Ingénierie des Matériaux Polymères, F-69621 Villeurbanne, France.*

S1. Characterisation of multifunctional polymer chains

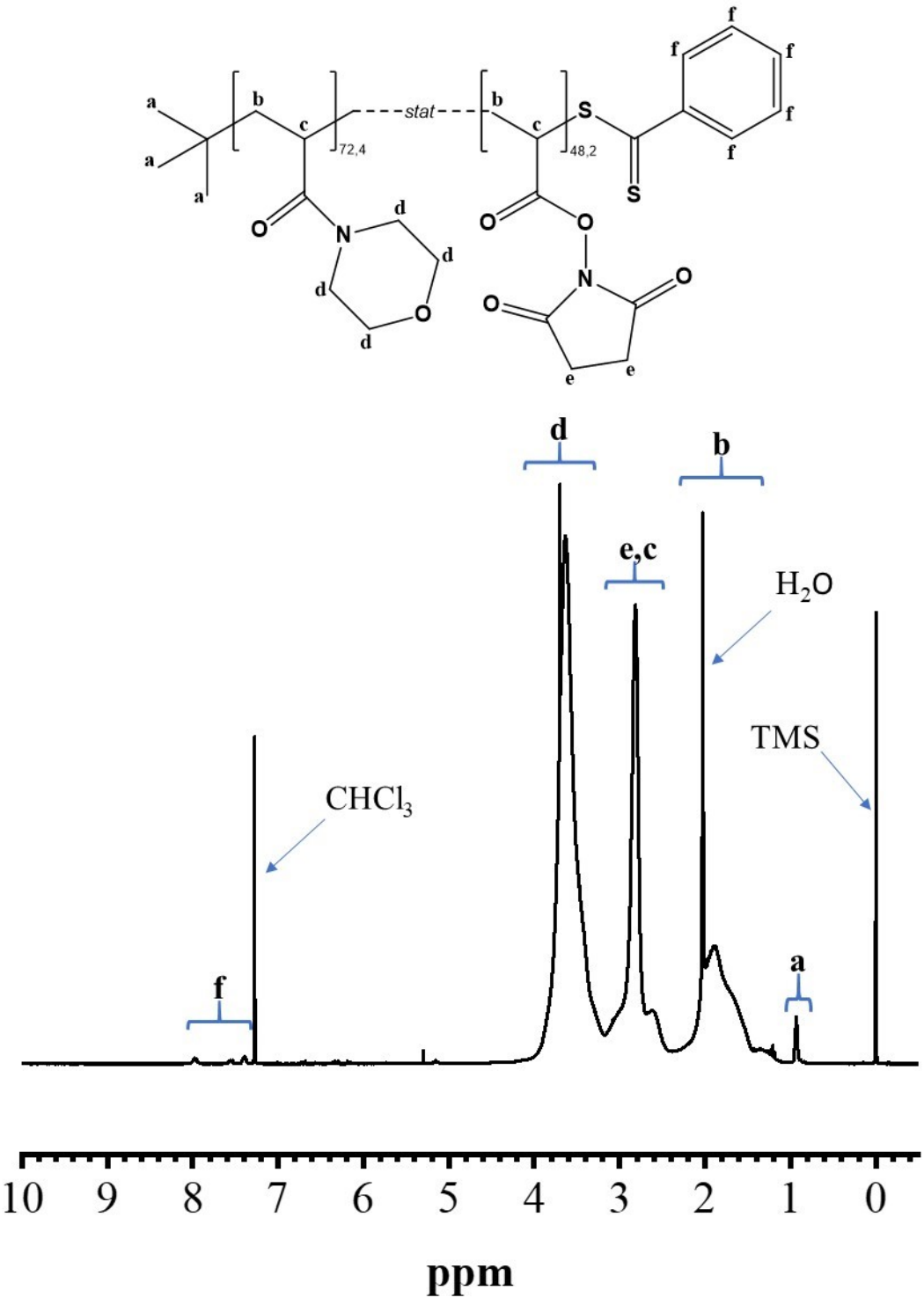

Figure S1. ^{1}H NMR spectrum of 19K P(NAM-*stat*-NAS) reactive polymer precursor before DBCO coupling (512 scans, 400 MHz, $CDCl_3$) along with the chemical formula of the polymer, showing to which protons each highlighted peak corresponds.

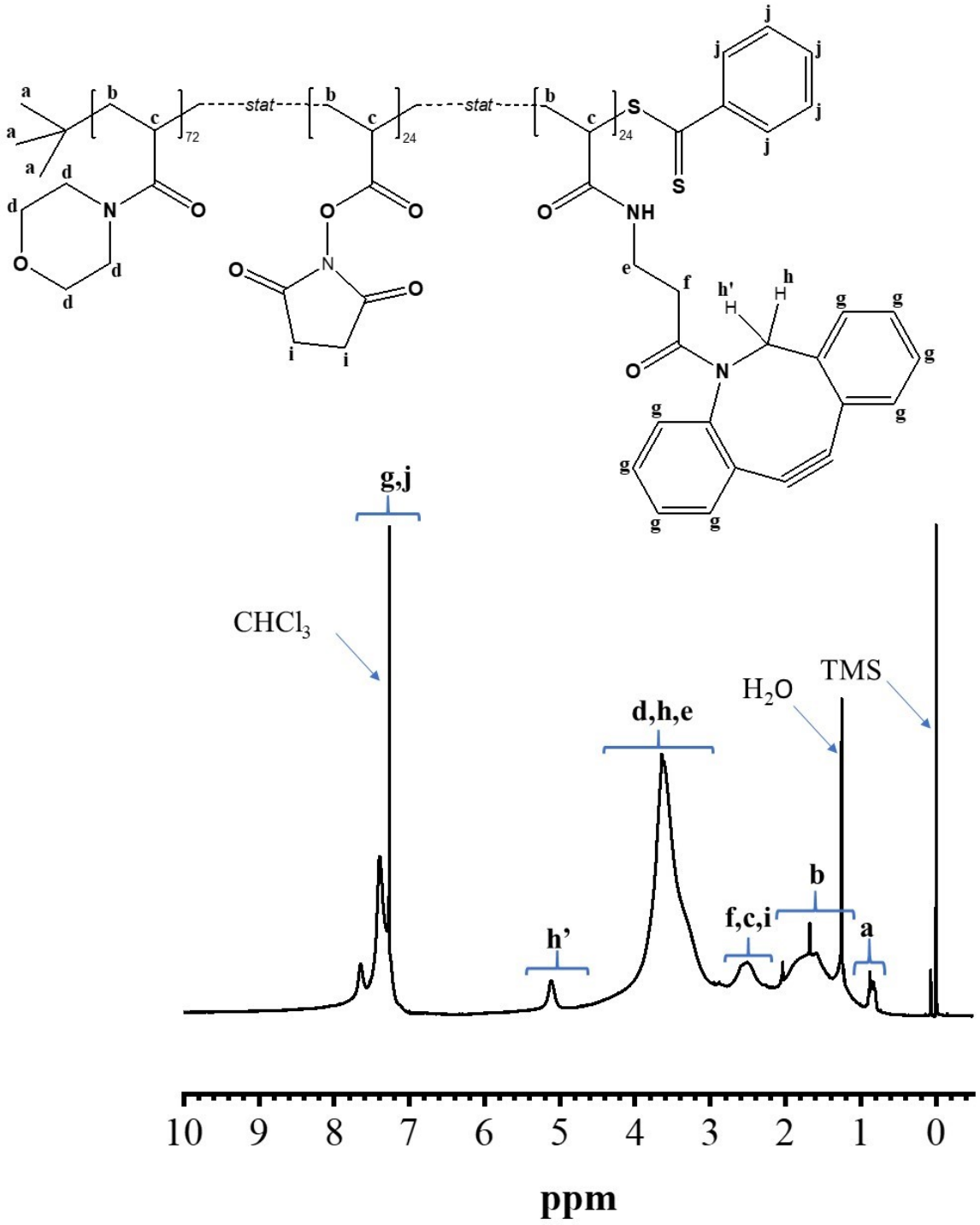

Figure S2. ^{1}H NMR spectrum of 19K-24DBCO polymer after purification by precipitation in diethyl ether and before hydrolysis (256 scans, 400 MHz, $CDCl_3$) along with the chemical formula of the polymer, showing to which protons each highlighted peak corresponds. DBCO coupling yield was determined by comparing the integrals corresponding proton noted h' at 5.1 ppm (fixed at 1) and protons noted (d,h,e) at 3-4.5 ppm (here 3.64).

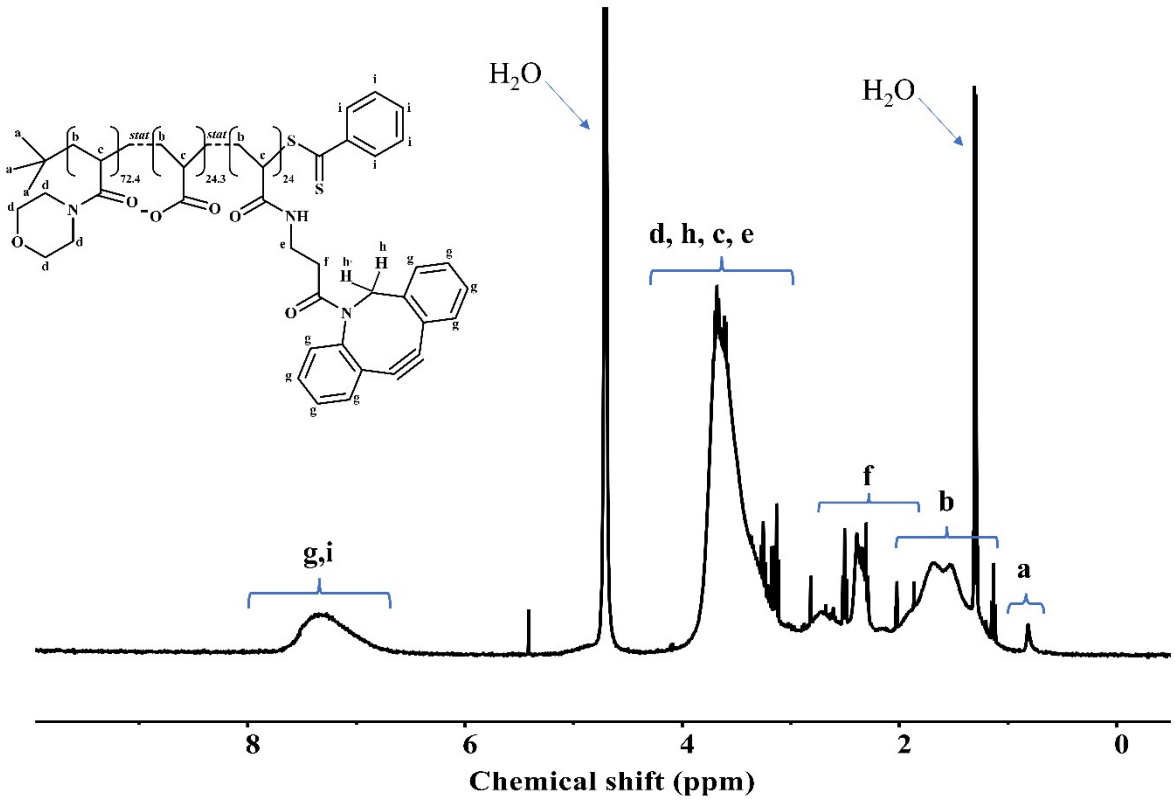

Figure S3. ^{1}H NMR spectrum of 19K-12DBCO polymer after purification by precipitation in diethyl ether and after hydrolysis of remaining NAS units (256 scans, 400 MHz, deuterated PBS) along with the chemical formula of the polymer, showing to which protons each highlighted peak corresponds. The small spikes in the NMR spectrum are associated with the small molecules, ions in PBS.

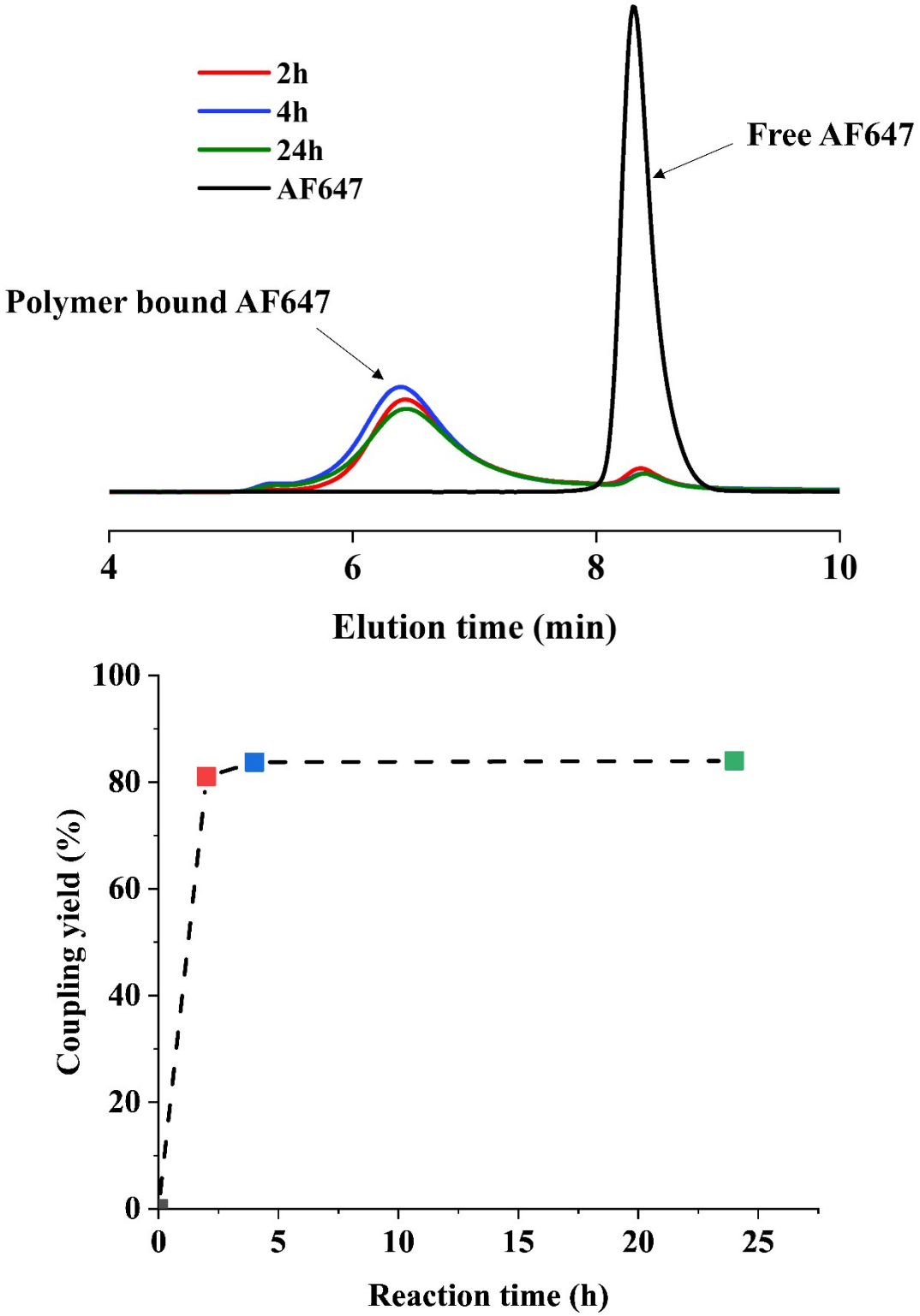

Figure S4. SPAAC coupling of AF647-N_3 fluorophore onto 19K-12DBCO polymer in PBS aqueous buffer followed by SEC-UV at 655 nm. AF647 fluorophore was rapidly coupled on the polymer (retention time between 5 to 8 min) compared to the free fluorophore (peak at 8.5 min retention time). SPAAC coupling yield was determined from the integration of the corresponding peak following the previously reported procedure[1].

S2. Physico-chemical characterisation of AuNCs

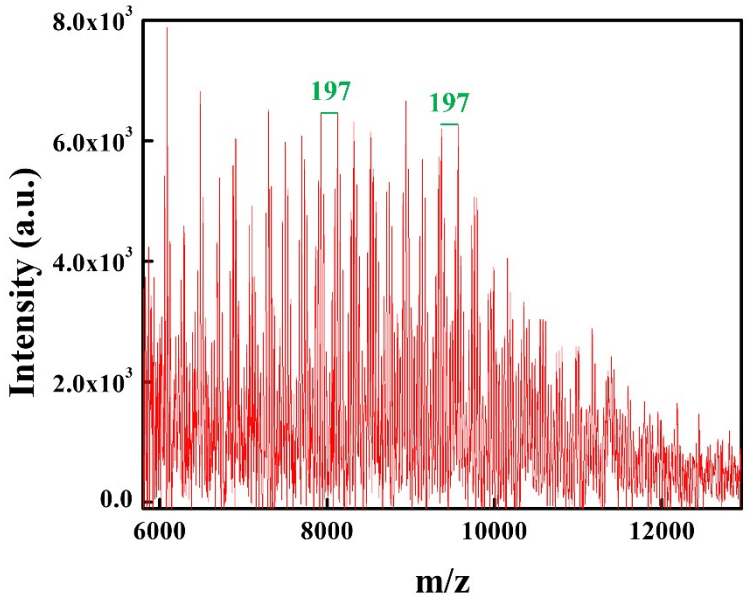

Figure S5. **MALDI-MS Characterisation of Au-PEGN$_3$** MALDI-MS in linear positive mode using HCCA matrix for Au-PEGN$_3$. The shift of mass m/z= 197 corresponds to the difference in number of gold atoms in the core.

Table S1. Table summarising the FTIR frequencies of Au-PEGN_3 experimental and theoretical values.

	Frequency (cm^{-1})		Type of vibration
	Experimental	**Theoretical**	
1.	3436	3450	O-H/ N-H stretching
2.	2969	2950	C-H stretching
3.	2361	2350	CO_2 stretching
4.	2131	2105	N_3 stretching
5.	1721	1733	C=O stretching
6.	1458	1452	C-N stretching
7.	1234	1233	C-H in-plane bending

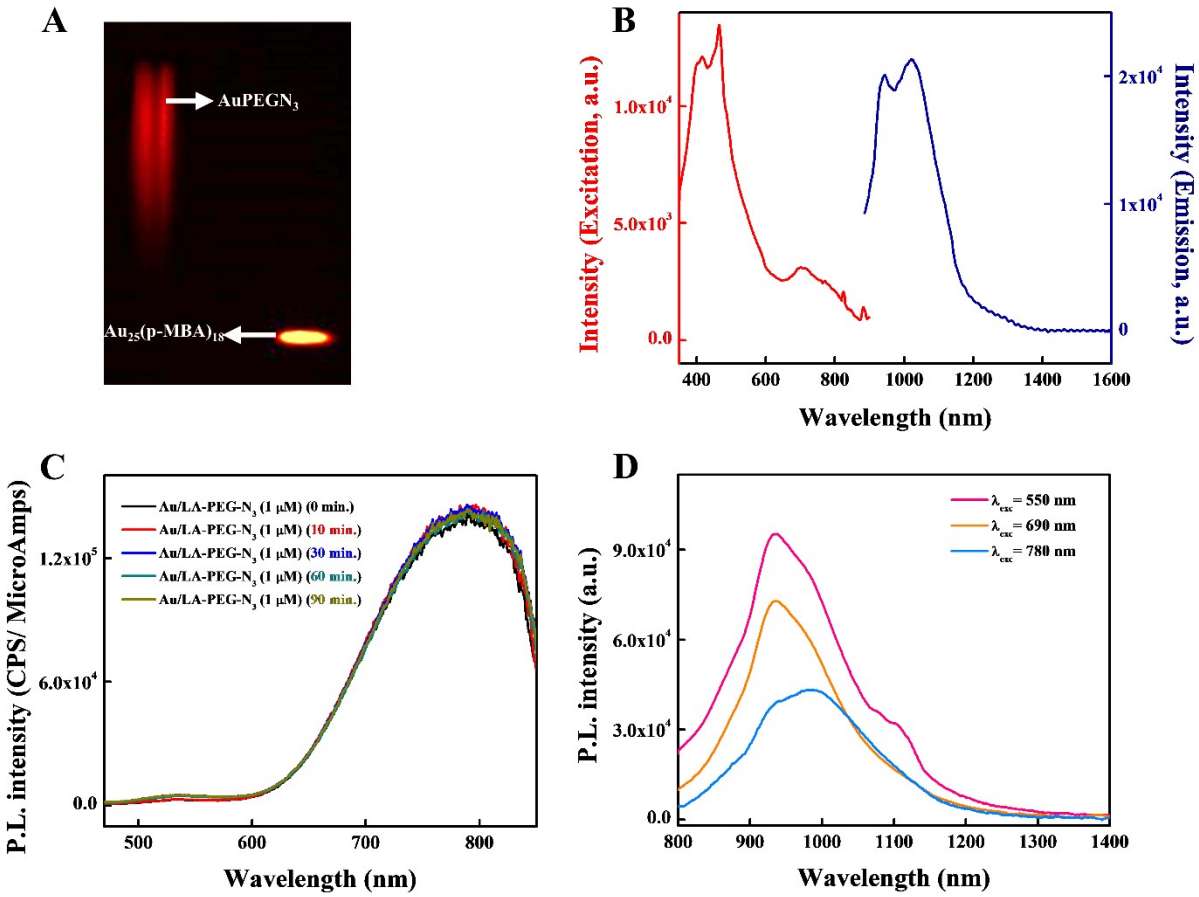

Figure S6. Characterization of luminescence properties of Au-PEGN$_3$ nanoclusters. (**A**) Polyacrylamide gel electrophoresis (PAGE) luminescence image of Au-PEGN$_3$ in comparison with atomically precise Au_{25}(p-MBA)$_{18}$ (p-MBA: para-mercaptobenzoic acid) under NIR excitation ($\lambda_{exc.}$= 808 nm) using long pass filter at 1064 nm. (**B**) The excitation ($\lambda_{em.}$ = 1000 nm), emission ($\lambda_{exc.}$= 808 nm) spectra of Au-PEGN$_3$ (1 μM) in PBS at 24°C. (**C**) The emission spectra ($\lambda_{exc.}$= 450 nm) showing the stability of Au-PEGN$_3$ (1 μM) over time in PBS. (**D**) The emission ($\lambda_{exc.}$= 550, 690 and 780 nm) spectra of Au-PEGN$_3$ (1 μM) in PBS at 24°C.

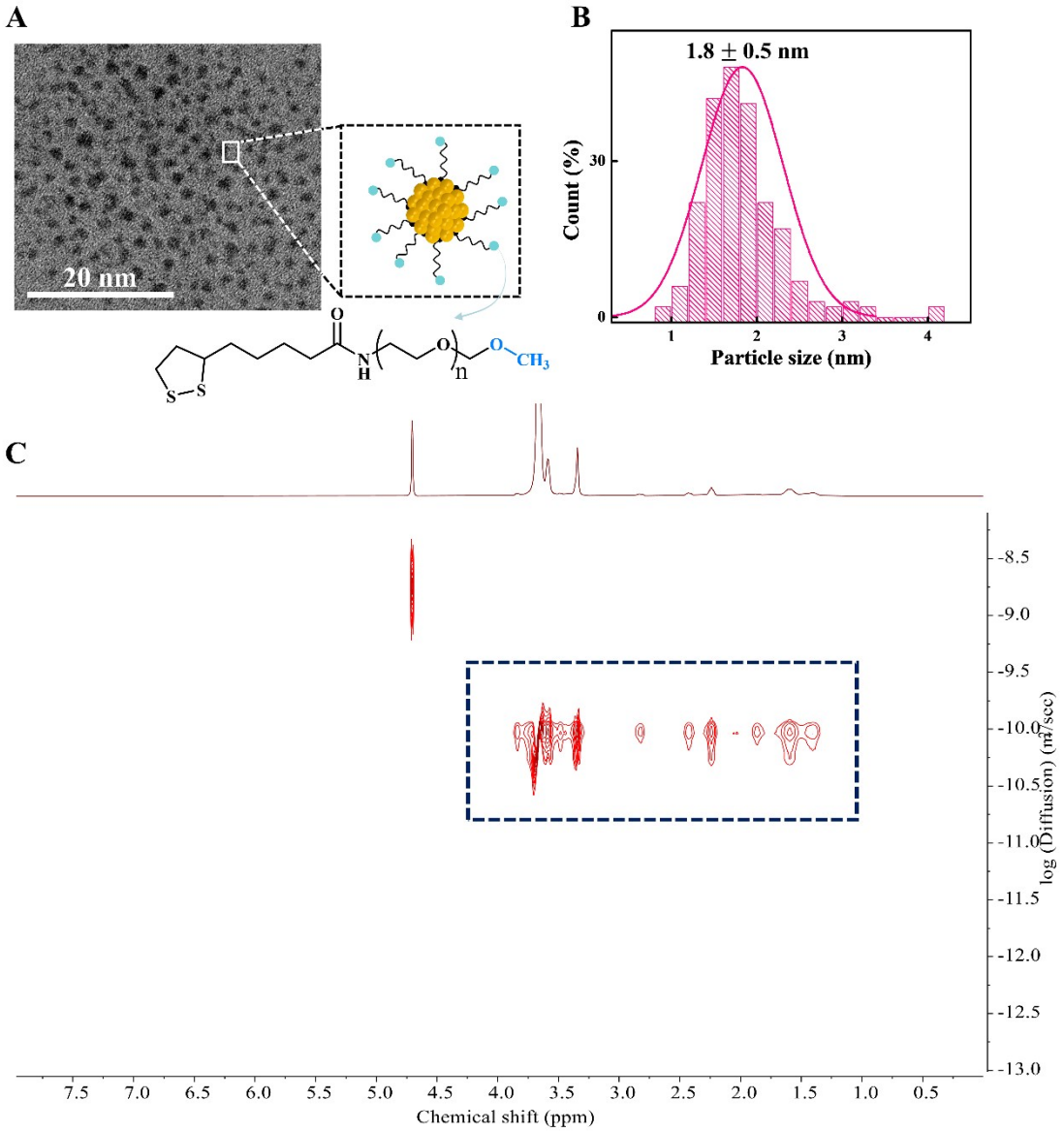

Cluster	D (m^2/sec)	R_H (nm)
AumPEG	$(7.0\pm0.1) \times 10^{-11}$	2.6 ± 0.2

Figure S7. **Characterization of Au-PEGOCH$_3$ nanoclusters**. (**A**) Characteristic TEM image of Au-PEGOCH$_3$ with the chemical structure of the stabilizing ligand LA-PEGOCH$_3$ (average number of PEG units, n = 10-14). (**B**) Average particle size distribution from TEM analysis using 220 particles. (**C**) The 1H-DOSY spectra of Au-PEGOCH$_3$, with the log (Diffusion) (m^2/sec) plotted *versus* the chemical shift (ppm). The measurements are performed in deuterated PBS at 298 K. The contour lines represent the signal intensity where each signal corresponds to a distinct chemical environment associated with the AuNC. Table shows the value of the diffusion coefficient (*D*, m^2/sec) and hydrodynamic diameter (R_H, nm), both as average ± SD, calculated from the Stokes−Einstein Equation (R_H is calculated from the average value of D assuming viscosity of deuterated PBS = 1.22×10^{-3} Pa·s).

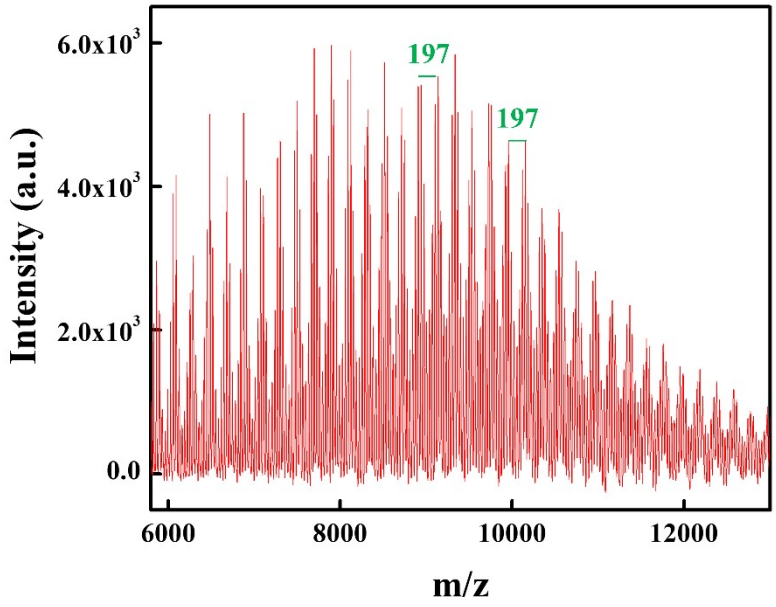

Figure S8. MALDI-MS Characterisation of Au-PEGOCH$_3$. MALDI-MS obtained in linear positive mode using HCCA matrix for Au-PEGOCH$_3$. The shift of mass m/z= 197 corresponds to the difference in number of gold atoms in the core.

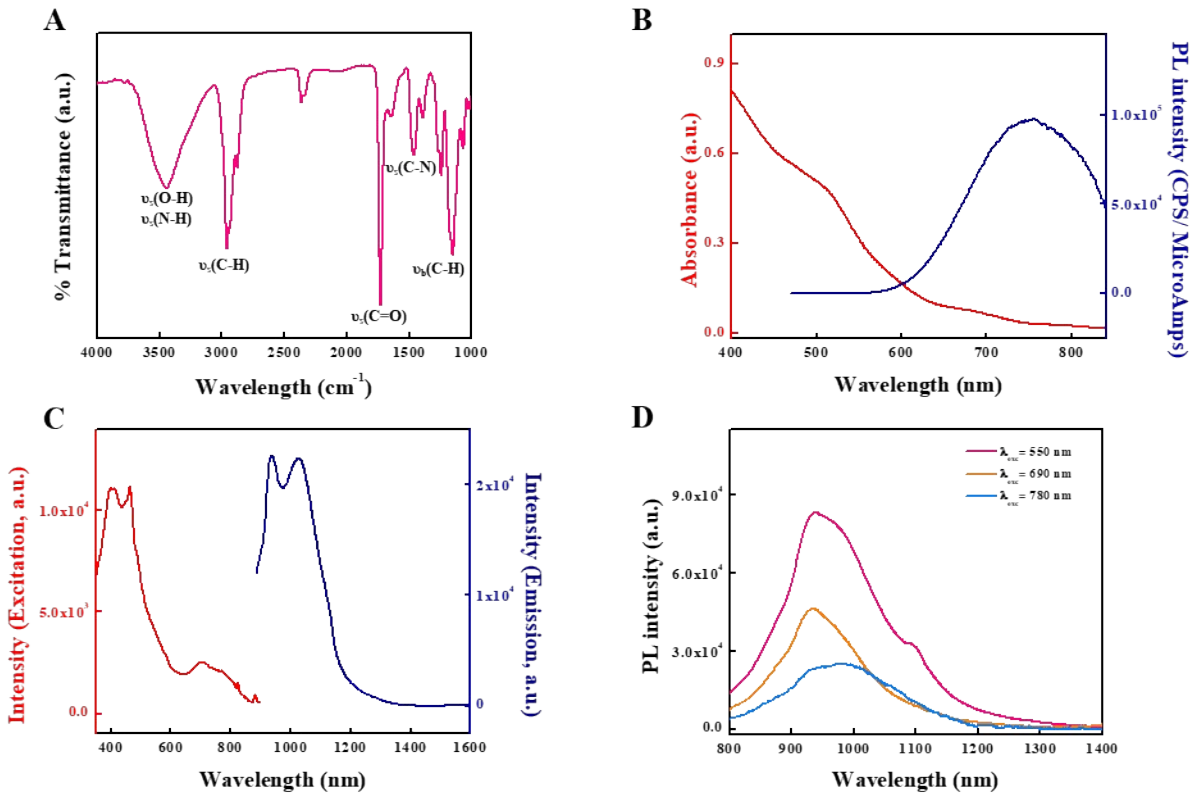

Figure S9. **Spectral properties of Au-PEGOCH$_3$ nanoclusters**. (**A**) The FT-IR spectra of freeze-dried Au-PEGOCH$_3$. (**B**) The absorbance and emission spectra ($\lambda_{exc.}$ = 450 nm) recorded for Au-PEGOCH$_3$ in PBS. (**C**) The excitation ($\lambda_{em.}$ = 1000 nm), emission ($\lambda_{exc.}$ = 808 nm) and (**D**) emission ($\lambda_{exc.}$ = 550, 690 and 780 nm) spectra recorded for Au-PEGOCH$_3$ in PBS. All the optical measurements are done at a concentration of 1 μM in PBS at 24°C.

S2.1. ^{1}H NMR spectral data.

The ligands used for the synthesis of AuNCs are commercial and the NMR characteristics were found as expected and after conjugation with the AuNCs major changes are observed in terms of chemical shifts, peak broadness and multiplicity. For instance, in case of Au-PEGN_3 (see **Section S2.1.1** and **S2.1.2**), all the methyl protons that are far from the ring exhibit signal broadening with no significant chemical shift difference between free and surface bound ligands, indicating these ligands are farthest from the gold surface and exhibits solution like behaviour relative to other protons[2]. The main changes are observed for the ring protons. The methyl protons are detectable with an upfield chemical shifts, while the ring protons close to S are not observed because of significant signal broadening and this further confirms that the ligand is attached to the gold surface via the dithiol ring with the azide groups extending out into the solution.

S2.1.1. LA-PEGN_3. ^{1}H NMR (400 MHz, D_2O): δ_H = 3.76-3.57 (broad, 26 H), 3.47-3.39 (t, 2H), 3.39-3.28 (t, 2H), 3.25-3.06 (m, 3H), 2.5-2.35 (m, 1H), 2.28-2.12 (t, 2H), 2.008-1.84 (m, 1H), 1.76-1.64 (m, 1H), 1.64-1.49 (m, 3H), 1.41-1.31 (m, 2H).

S2.1.2. Au-PEGN_3. ^{1}H NMR (400 MHz, D_2O): δ_H = 3.83-3.60 (broad, 29 H), 3.53-3.42 (t, 2H), 3.42-3.30 (t, 2H), 2.51-2.36 (broad, 1H), 2.34-2.14 (t, 2H), 2.10-1.95 (broad, 1H), 1.77-1.64 (broad, 2H), 1.67-1.49 (broad, 3H), 1.44-1.33 (broad, 2H).

S2.1.3. LA-PEGOCH_3. ^{1}H NMR (400 MHz, D_2O): δ_H 3.75-3.49 (broad, 50 H), 3.38-3.23 (broad, 4H), 3.23-3.09 (m, 3H), 2.48-2.37 (m, 1H), 2.29-2.16 (t, 2H), 1.98-1.87 (m, 1H), 1.75-1.64 (m, 2H), 1.64-1.49 (m, 2H), 1.41-1.31 (m, 2H).

S2.1.4. Au-PEGOCH_3. ^{1}H NMR (400 MHz, D_2O): δ_H 3.81-3.52 (broad, 55 H), 3.42-3.27 (broad, 4H), 2.51-2.40 (broad, 1H), 2.30-2.18 (t, 2H), 2.07-1.89 (broad, 1H), 1.76-1.66 (broad, 2H), 1.66-1.52 (broad, 2H), 1.42-1.31 (broad, 2H).

S3. Characterization of nanocluster/polymer conjugation by QCM-D

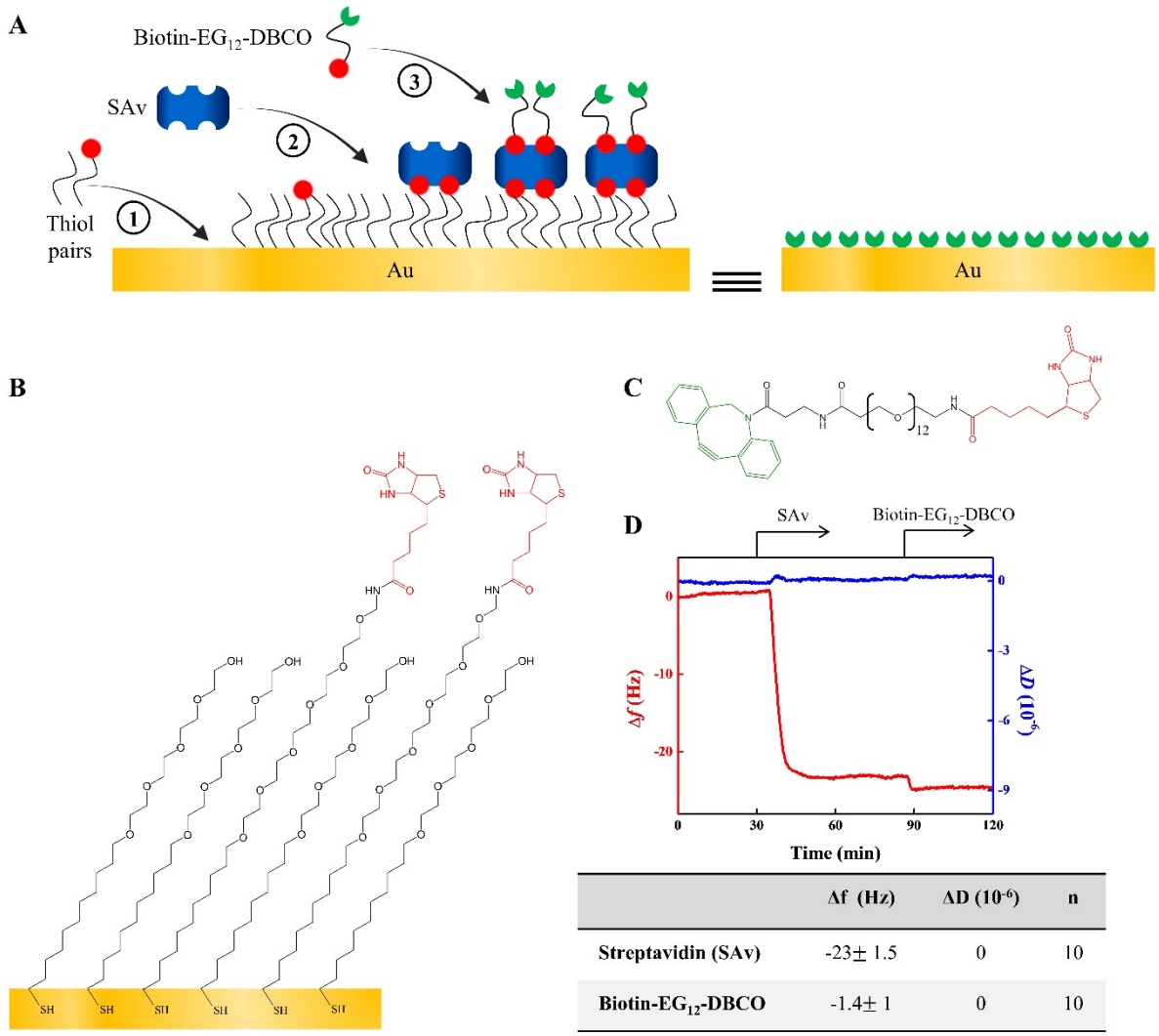

	Δf (Hz)	ΔD (10^{-6})	n
Streptavidin (SAv)	-23± 1.5	0	10
Biotin-EG$_{12}$-DBCO	-1.4± 1	0	10

Figure S10. **Functionalization of planar gold surfaces with DBCO**. (**A**) Schematic representation of the main steps of surface functionalization for the generation of DBCO monolayer: ① 10% biotinylated SAMs formed through thiol/gold chemistry, ② SAv monolayer formation and ③ DBCO monolayer formation using biotin-EG$_{12}$-DBCO. (**B**) Chemical structure of the thiols HS-(CH$_2$)$_{11}$-EG$_4$-OH and HS-(CH$_2$)$_{11}$-EG$_6$-biotin. (**C**) Chemical structure of biotin-EG$_{12}$-DBCO. (**D**) The QCM-D response, Δf (red) and ΔD (blue) (overtone i=7) shifts recorded during the exposure of 10%-biotinylated SAMs to SAv, followed by the injection of biotin-EG$_{12}$-DBCO. The corresponding frequency and dissipation changes after rinsing with the working buffer are summarized in the table below. Values represent the mean ± SEM from n measurements, where n is the number of experiments treated. The solutions in contact with the surfaces at different time points are indicated by arrows on the top of the QCM-D graph.

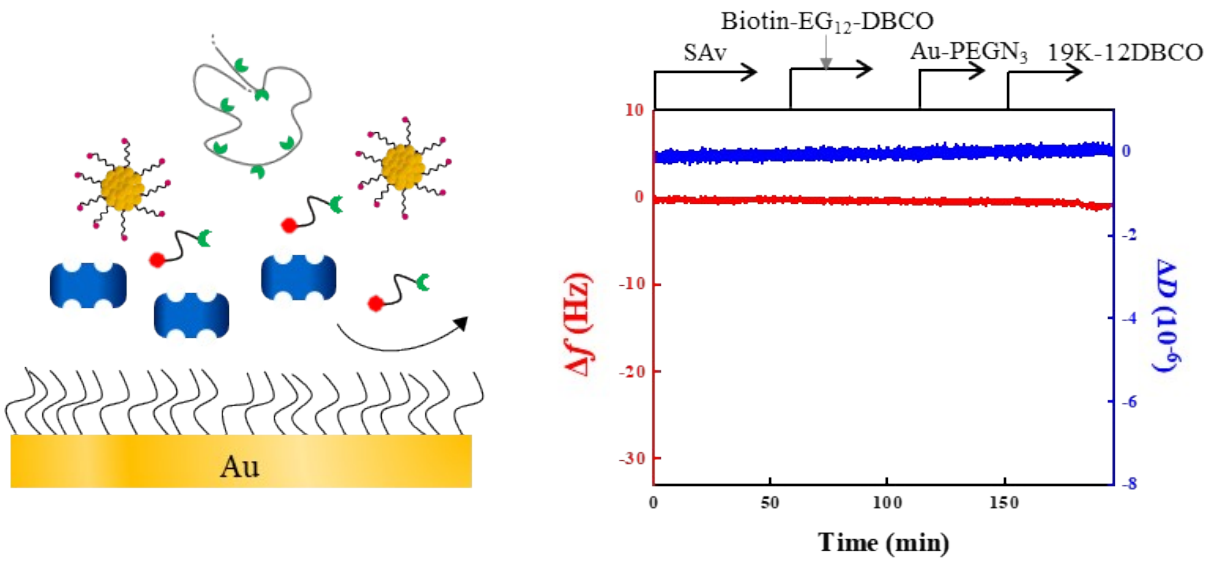

Figure S11. **QCM-D control experiments to confirm specificity:** Schematic representation with respective QCM-D profiles (Δf and ΔD, overtone i=7) showing the absence of interactions of 0% biotinylated SAMs with SAv, biotin-EG_{12}-DBCO, Au-$PEGN_3$ and 19K-12DBCO. The arrows at the top of QCM-D profile indicate the start and incubation duration with each sample as specified, while a working buffer (PBS) was flushed over the sensor surface during the remaining periods.

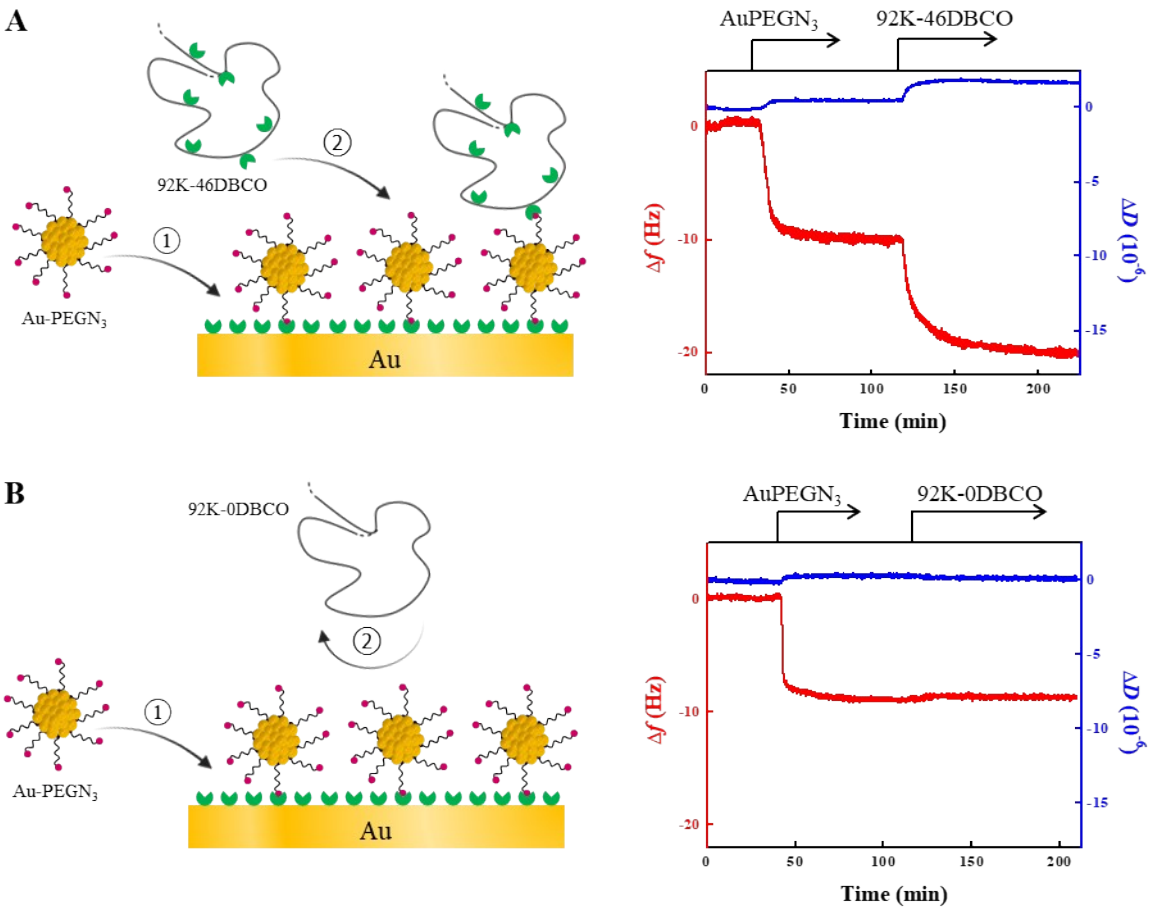

C

	Δf (Hz)	ΔD (10^{-6})	n
Au-PEGN$_3$	-10±1.5	0.8±0.5	11
92K-46DBCO	-10±1	1.2±1	2
92K-0DBCO	0	0	2

Figure S12. QCM-D characterization of the specificity of bioorthogonal conjugation between Au-PEGN$_3$ nanoclusters and 92K-46DBCO polymers. **(A)** Schematic representation with respective Δ*f* (red) and Δ*D* (blue) shifts (overtone i=7) obtained for the subsequent addition of Au-PEGN$_3$ (1 μM) and 92K-46DBCO (10 μM) to the DBCO-functionalized surfaces. **(B)** The schematic showing the absence of interaction between the Au-PEGN$_3$ and 92K-0DBCO concluded based on the absence of QCM-D response during the exposure of layer (formed by injection of 1 μM Au-PEGN$_3$) to 92K-0DBCO (10 μM). The arrows at the top of QCM-D profiles indicate the start and incubation duration with each sample as specified, while a working buffer (PBS) was flushed over the sensor surface during the remaining periods. (C) Table summarizing the corresponding Δ*f* and Δ*D* for both experiments, where n is the number of experiments treated.

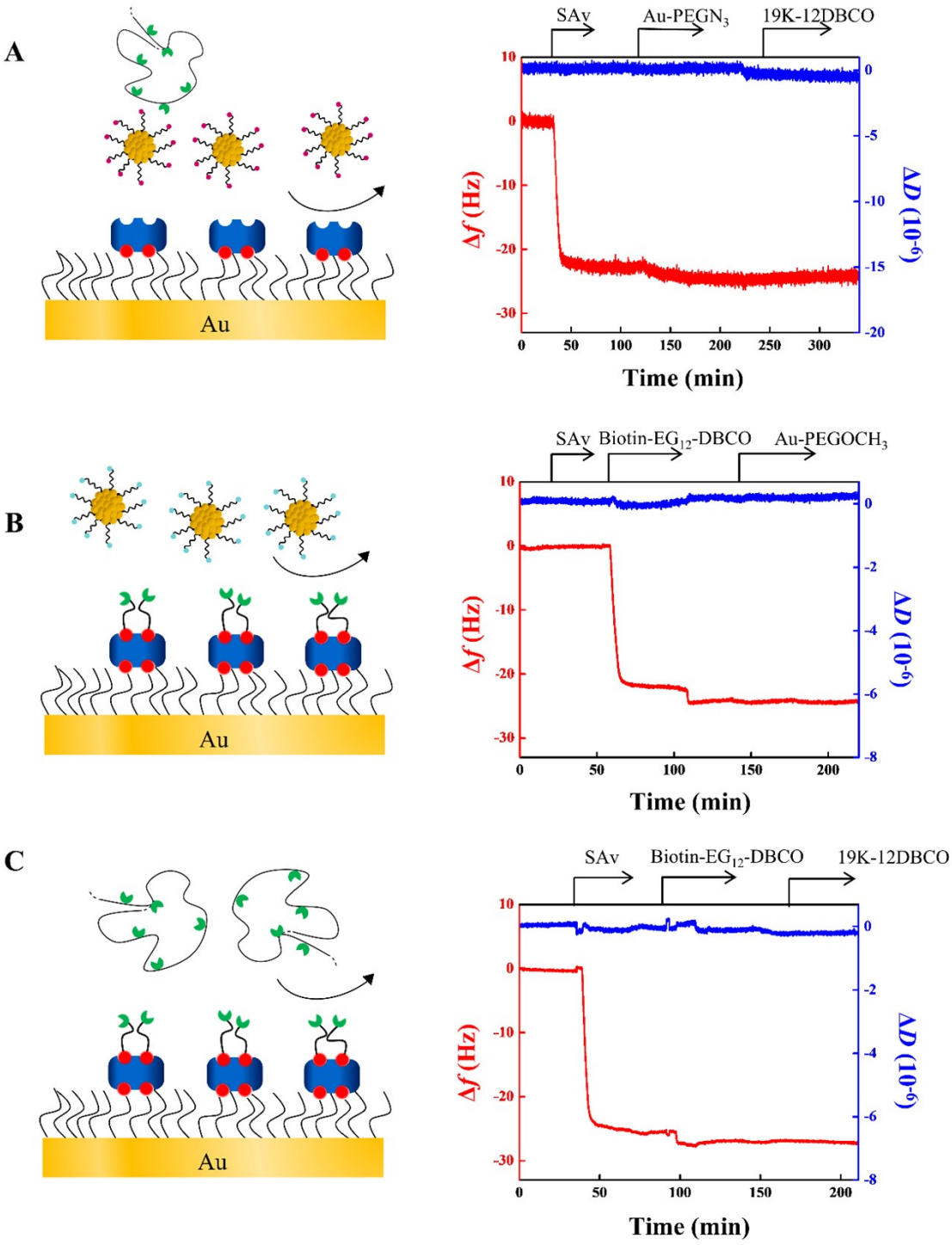

Figure S13. **Additional QCM-D control experiments to confirm specificity of biorthogonal conjugation.** Schematic representation with respective QCM-D profiles (Δf and ΔD, overtone i=7) showing the absence of interactions of **(A)** SAv layer with Au-PEGN$_3$ and 19K-12DBCO, **(B)** DBCO layer with Au-PEGOCH$_3$, and **(C)** DBCO layer with 19K-12DBCO. The concentrations of Au-PEGN3 and 19K-12DBCO solutions are 1 and 10 μM respectively. Similar results are obtained with other polymeric systems (19K-24DBCO, 92K-46DBCO and 92K-92DBCO) and different Au-PEGN$_3$ concentrations (10 and 40 μM). The arrows at the top of QCM-D profile indicate the start and incubation duration with each sample as specified, while a working buffer (PBS) was flushed over the sensor surface during the remaining periods.

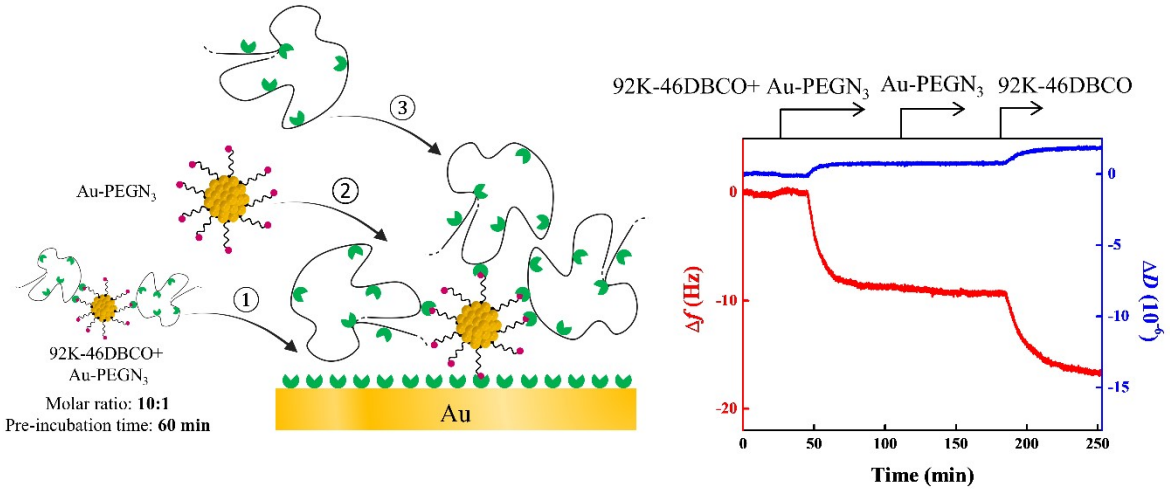

	Δf (Hz)	ΔD (10^{-6})	n
92K-46DBCO+ Au-PEGN$_3$	-9±1	0.9±0.5	11
Au-PEGN$_3$	0	0	2
92K-46DBCO	-7.4±0.5	1.2±0.3	2

Figure S14. QCM-D characterization of the efficiency of bioorthogonal conjugation between Au-PEGN$_3$ nanoclusters and 92K-46DBCO polymers. Schematic representation of interactions studied on DBCO-coated surfaces and reflected in Δ*f* (red) and Δ*D* (blue) shifts (overtone i=7) during the injection of the mixture of 92K-46DBCO and Au-PEGN$_3$ (at polymer : AuNC molar ratio of 10:1) pre-incubated during 60 minutes, followed by the subsequent injection of Au-PEGN$_3$ (1 μM) and 92K-46DBCO (10 μM). The arrows at the top of the QCM-D profile indicate the start and incubation duration with each sample as specified, while a working buffer (PBS) was flushed over the sensor surface during the remaining periods. Table summarizing the corresponding Δ*f* and Δ*D* for all steps, where n is the number of experiments treated.

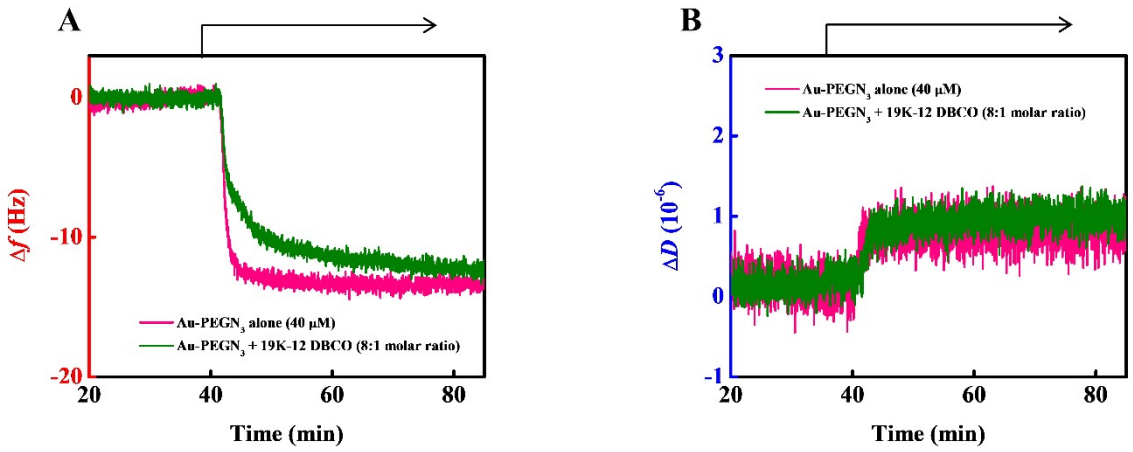

	Δf (Hz)	ΔD (10^{-6})
Au-PEGN$_3$ (40 μM)	-13.4	0.82
19K-12DBCO (5 μM)+ **Au-PEGN$_3$** (40 μM) (polymer: AuNC molar ratio= 1:8)	-12.1	1.02

Figure S15. QCM-D monitoring of (**A**) Δ*f* and (**B**) Δ*D* shifts during the injection of Au-PEGN$_3$ alone (pink, 40 μM) and a mixture of 19K-12DBCO and Au-PEGN$_3$ (green, at polymer: AuNC molar ratio of 1:8; excess cluster condition, [polymer]= 5 μM and [AuNC]= 40 μM). Table summarizing the corresponding Δ*f* and Δ*D* for both steps, where n is the number of experiments treated.

S4. Characterization of optical properties of nanocluster/polymer conjugates

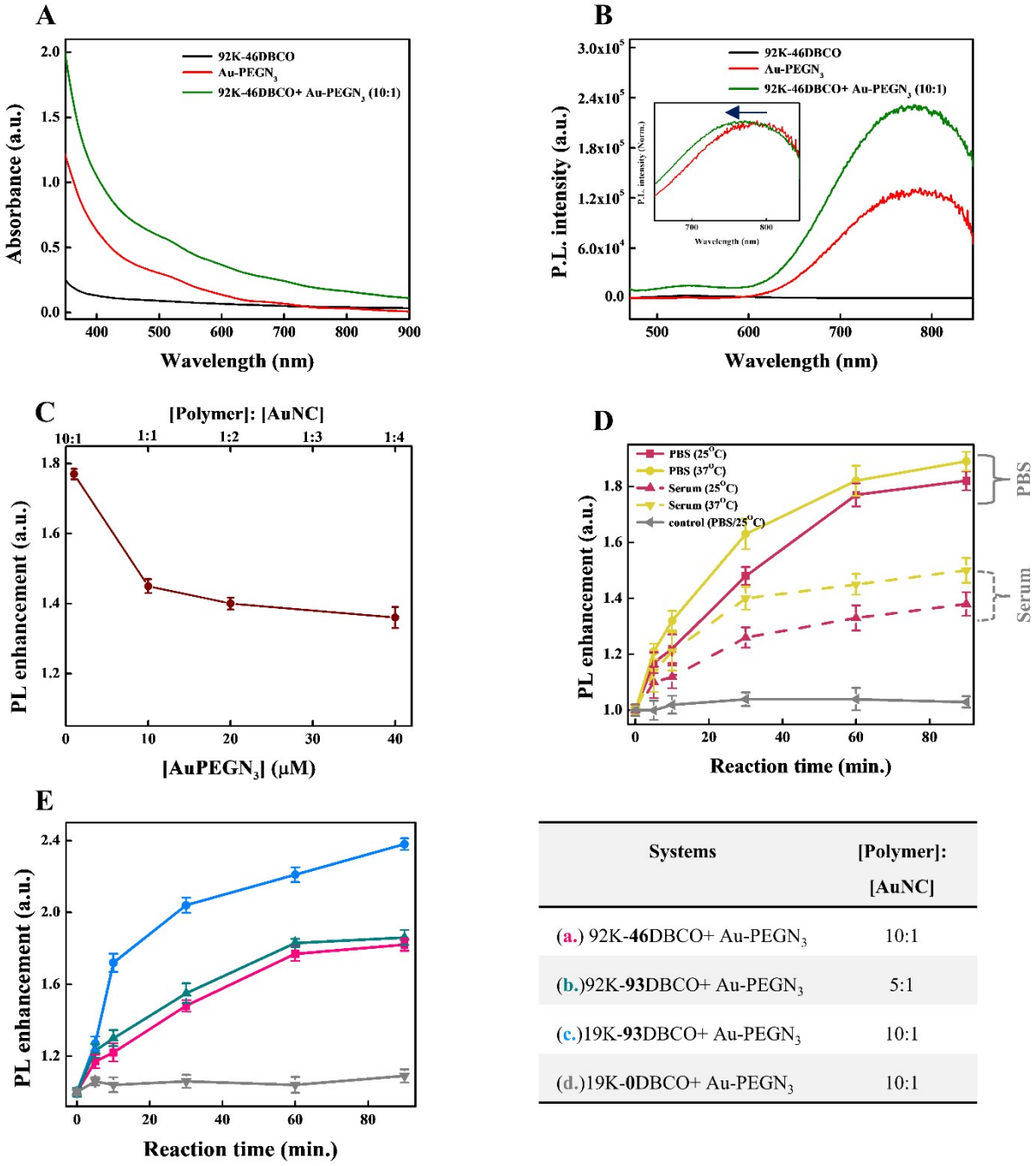

Systems	[Polymer]: [AuNC]
(a.) 92K-**46**DBCO+ Au-PEGN$_3$	10:1
(b.)92K-**93**DBCO+ Au-PEGN$_3$	5:1
(c.)19K-**93**DBCO+ Au-PEGN$_3$	10:1
(d.)19K-**0**DBCO+ Au-PEGN$_3$	10:1

Figure S16. Optical properties of nanocluster/polymer conjugates. The characteristic (**A**) absorbance and (**B**) PL emission spectra (λ_{exc} = 450 nm) of 92K-46DBCO (black), Au-PEGN$_3$ (red) and the mixture of 92K-46DBCO : Au-PEGN$_3$ at 10:1 ratio (green) (concentration of Au-PEGN$_3$ and 92K-46DBCO used are 1 and 10 μM, respectively). Inset in (B) shows the blue shift (~18 ± 2 nm, n=3) of the PL emission maximum upon mixing Au-PEGN$_3$ with 92K-46DBCO. (**C**) PL enhancement recorded for Au-PEGN$_3$: 92K-46DBCO mixtures at different Au-PEGN$_3$ concentrations keeping 92K-46DBCO concentration fixed to 10 μM. Absorbance and PL emission experiments were done at 25°C in PBS; all mixtures were pre-incubated for 1 hour. (**D**) PL enhancement recorded

for the mixtures of 92K-46DBCO: Au-PEGN$_3$ at 10:1 ratio as a function of pre-incubation time in PBS or DMEM with 10% serum at 25 (yellow) or 37°C (red); [Au-PEGN$_3$] = 1 μM, [92K-46DBCO] = 10 μM, number of experiments averaged = 2. Control system based on Au-PEGOCH$_3$ is shown in gray. (**E**) The PL enhancement for the mixtures of 92K-46DBCO or 92K-93DBCO with Au-PEGN$_3$ at tunable ratio and DBCO density plotted as a function of their pre-incubation time; experiments are done at 25°C in PBS (number of experiments averaged = 2). Table summarizing the studied mixtures is shown next to the graph.

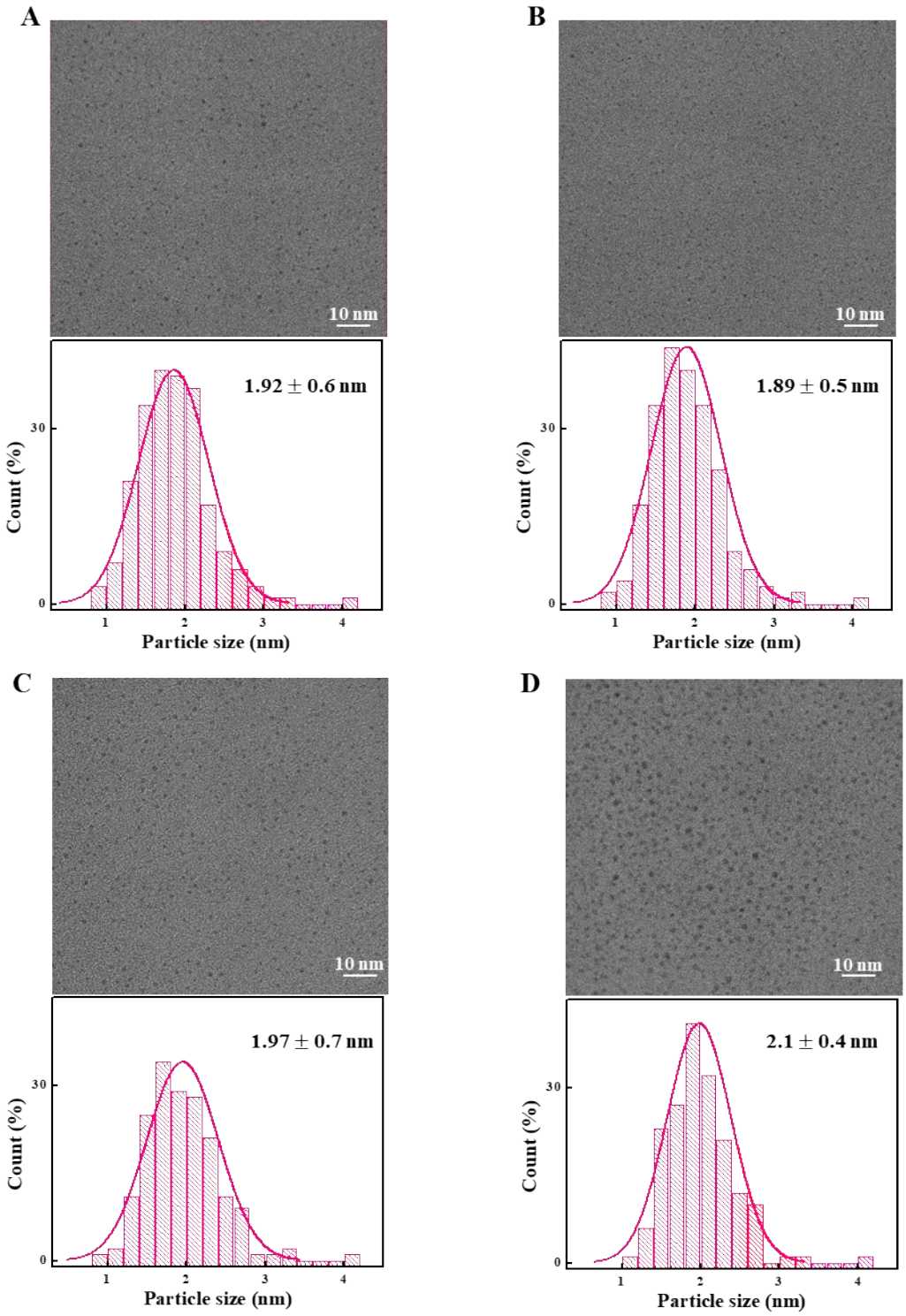

Figure S17. TEM images of Au-PEGN$_3$ conjugated with DBCO-modified polymers at different ratios and tunable DBCO density: (**A**) 19K-12DBCO : Au-PEGN$_3$ = 10 : 1, (**B**) 19K-12DBCO : Au-PEGN$_3$ = 1: 1, (**C**) 19K-24DBCO : Au-PEGN$_3$ = 10 : 1, (**D**) 19K-0DBCO : Au-PEGN$_3$ = 10 : 1.

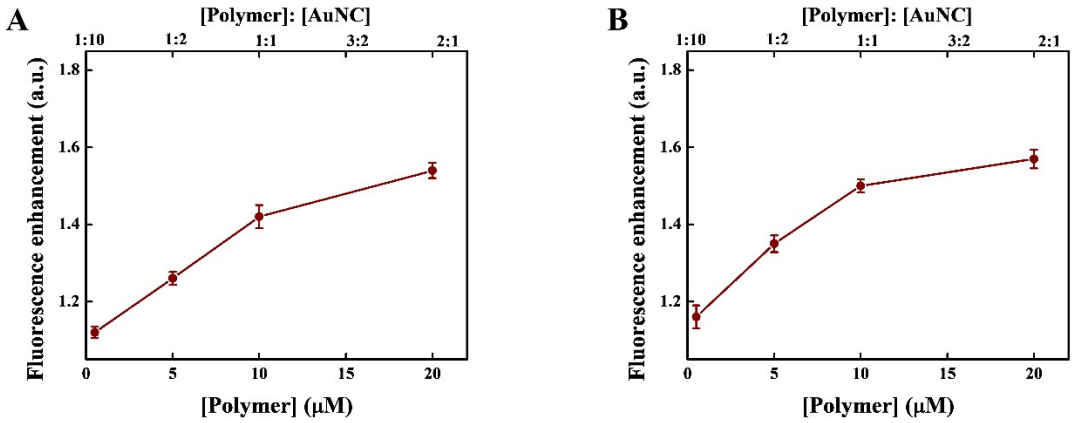

Figure S18. Impact of polymer concentration on bioorthogonal reaction: PL enhancement recorded for (**A**) Au-PEGN$_3$: 19K-12DBCO and (**B**) Au-PEGN$_3$: 92K-46DBCO mixtures at different polymer concentrations keeping Au-PEGN$_3$ concentration fixed to 10 μM. PL emission experiments were done at 25°C in PBS at λ_{exc} = 450; all mixtures were pre-incubated for 1 hour.

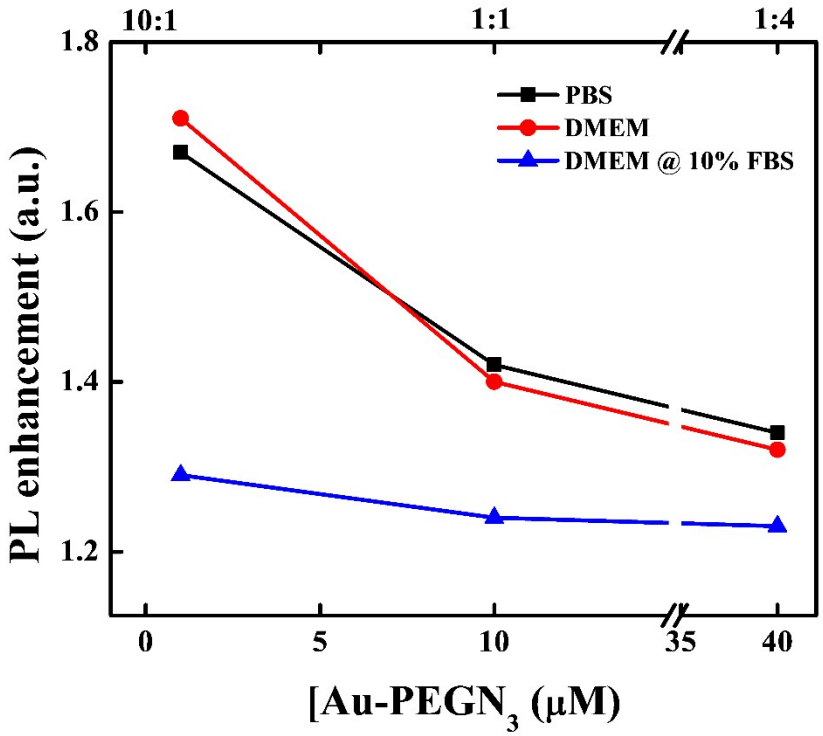

Figure S19. Impact of solvent (PBS, DMEM and DMEM with 10% Serum) on biorthogonal reaction: PL enhancement recorded for Au-PEGN$_3$: 19K-12DBCO mixtures at different polymer concentrations, keeping polymer concentration fixed to 10 μM. PL emission experiments were done at 25°C in PBS, DMEM and DMEM with 10% serum at λ_{exc} = 450; all mixtures were pre-incubated for 1 hour.

REFERENCES

1. C. Cepraga, T. Gallavardin, S. Marotte, P.-H. Lanoë, J.-C. Mulatier, F. Lerouge, S. Parola, M. Lindgren, P. L. Baldeck, J. Marvel, O. Maury, C. Monnereau, A. Favier, C. Andraud, Y. Leverrier and M.-T. Charreyre, *Polymer Chemistry*, 2013, **4**, 61-67.
2. O. Kohlmann, W. E. Steinmetz, X.-A. Mao, W. P. Wuelfing, A. C. Templeton, R. W. Murray and C. S. Johnson, *The Journal of Physical Chemistry B*, 2001, **105**, 8801-8809.